


# Sign switching of superexchange mediated by a few electrons in a nonuniform magnetic field

Guo Xuan Chan  and Xin Wang \*

*Department of Physics, City University of Hong Kong, Tat Chee Avenue, Kowloon, Hong Kong SAR, China  
and City University of Hong Kong Shenzhen Research Institute, Shenzhen, Guangdong 518057, China*

 (Received 6 April 2022; accepted 8 August 2022; published 19 August 2022)

Long-range interaction between distant spins is an important building block for the realization of a large quantum-dot network in which couplings between pairs of spins can be selectively addressed. Recent experiments on the coherent oscillation of logical states between remote spins facilitated by intermediate electron states were the first step for large-scale quantum information processing. Reaching this ultimate goal requires extensive studies on the superexchange interaction in different quantum-dot spatial arrangements and electron configurations. Here, we consider a linear triple quantum dot with two antiparallel spins in the outer dots forming the logical states while varying numbers of electrons in the middle dot form a mediator, which facilitates the superexchange interaction. We show that the superexchange is enhanced when the number of mediating electrons increases. In addition, we show that forming a four-electron triplet in the mediator dot further enhances the superexchange strength. Our work can be a guide to scale up the quantum-dot array with controllable and dense connectivity.

DOI: [10.1103/PhysRevA.106.022420](https://doi.org/10.1103/PhysRevA.106.022420)

## I. INTRODUCTION

Early studies of semiconductor quantum-dot qubits, both experimental [1–24] and theoretical [25–37], mostly focused on interactions between neighboring electron spins. Approaches to harness nonproximal exchange interaction between distant spins are critical for achieving efficient non-local quantum operations, as increased connectivity leads to smaller quantum circuit depth [38]. Current implementations of long-range interaction between spins include capacitive coupling [14,39–42], photon-mediated interactions [43–51], and electron shuttling [52–57]. The former two schemes introduce coupling to the charge degree of freedom; hence, they are prone to decoherence by charge noise [14,40,47], while the latter method requires a relatively complex operation and coordination of the gate voltages to perform electron shuttling adiabatically [55]. An alternative method to have exchange interactions between remote spins is to enable a virtual exchange through a mediator, termed superexchange [38,58–63]. Current experimental progress has demonstrated coherent superexchange interaction with the mediator being an empty [61], singly occupied [58], or multielectron [60] quantum dot. Among different superexchange coupling schemes, implementing a multielectron quantum dot or dot chain is of interest because it has been shown theoretically that a larger number of electrons occupying the mediator leads to stronger superexchange interaction [64]. In addition, current works mostly focus on a spinless multielectron mediator [59,60,62,64], leaving the effect of the nonzero spin state formed in the mediator or a larger number of electrons occupying the mediator unanswered. In this paper, we explore, using configuration-interaction (CI) calculations, the effect on the superexchange in a linear triple-quantum-dot (TQD)

system with the mediator occupied by two or four electrons. Specifically, we compare three different cases for the mediator (summarized in Fig. 1): Case (i) is a spinless two-electron state. Case (ii) is a spin-1 four-electron state. Case (iii) is a spinless four-electron state. We have found that in contrast to the spinless two-electron mediator, which yields positive superexchange energy, the spinless four-electron mediator results in negative superexchange, with stronger magnitude. Furthermore, if a larger perpendicular magnetic field is applied to the outer two dots in a TQD device compared to the inner dot, for a spin-1 four-electron mediator, the superexchange, denoted as  $J$ , is negative for a moderate magnetic field but switches to a positive value for a much larger magnetic field, with  $J$  in the former case yielding a larger magnitude than the latter.

This paper is organized as follows: In Sec. II, the model and methods are provided. In Sec. III A, we evaluate the two- and four-electron systems in the mediator dot for different perpendicular magnetic field strengths, including the energy and total spin of the ground state. In Sec. III B, we present and compare the values of superexchange energy for different types of mediators, as shown in Fig. 1. We summarize our results in Sec. IV. The Appendixes give more details on the leakage estimation for the superexchange mediated by a triplet state (Appendix A), explicit expressions of the eigenstates written in the Slater determinants formed by Fock-Darwin orbitals (Appendix B), and additional results for zero external magnetic field (Appendix C).

## II. MODEL AND METHODS

We consider an  $N$ -electron system described by the Hamiltonian

$$H = \sum_{j=1}^N h_j + \sum_{j<k} \frac{e^2}{\epsilon |\mathbf{r}_j - \mathbf{r}_k|}, \quad (1)$$

\*x.wang@cityu.edu.hk

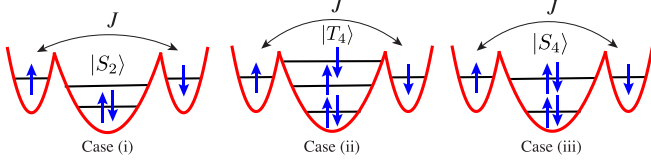


FIG. 1. Three different electron configurations studied in this work. Case (i): Two electrons in the mediator (middle dot) form a singlet ( $S = 0$ ), where  $S$  is the total spin. Case (ii): Four electrons in the mediator form a triplet ( $S = 1$ ). Case (iii): Four electrons in the mediator form a singlet ( $S = 0$ ).  $J$  is the superexchange energy between distant spins in the outer dots.

with the single-particle Hamiltonian  $h_j$  being

$$h_j = \frac{(-i\hbar\nabla_j + \frac{e\mathbf{A}_j}{c})^2}{2m^*} + V(\mathbf{r}_j) + g^*\mu_B\mathbf{B}_j \cdot \mathbf{S}_j, \quad (2)$$

where  $\mathbf{r}_j = x_j\hat{\mathbf{x}} + y_j\hat{\mathbf{y}}$  indicates the position of the  $j$ th electron with spin  $\mathbf{S}_j$  experiencing a perpendicular magnetic field  $\mathbf{B}_j = B_j\hat{\mathbf{z}}$ .  $\mathbf{A}_j$  is the vector potential corresponding to  $\mathbf{B}_j$ , and  $m^*$  is the effective mass, taken to be 0.067 electron mass in GaAs. In this work,  $V(\mathbf{r})$  describes the confinement potential of a TQD, modeled as (see Fig. 2)

$$V(\mathbf{r}) = \begin{cases} \frac{1}{2}m^*\omega_L^2(\mathbf{r} - \mathbf{R}_L)^2 & x < -x'_0, \\ \frac{1}{2}m^*\omega_M^2(\mathbf{r} - \mathbf{R}_M)^2 + \Delta & -x'_0 < x < x'_0, \\ \frac{1}{2}m^*\omega_R^2(\mathbf{r} - \mathbf{R}_R)^2 & x > x'_0. \end{cases} \quad (3)$$

Note that Eq. (3) defines the confining potential of circular quantum dots [65]. Here,  $\mathbf{R}_L = (-x_0, 0)$ ,  $\mathbf{R}_M = (0, 0)$ , and  $\mathbf{R}_R = (x_0, 0)$  are the minima of the three parabolic wells, representing three dots labeled L (left), M (middle), and R (right), respectively.  $\omega_L$ ,  $\omega_M$ , and  $\omega_R$  and  $B_L$ ,  $B_M$ , and  $B_R$  are the confinement strengths and the magnetic field at dots L, M, and R, respectively. The confinement strengths are set as  $\hbar\omega_L = \hbar\omega_R = 7.28$  meV,  $\hbar\omega_M = 3.64$  meV [64,66], while the magnetic field varies, which will be explained in the following sections. The potential cuts,  $-x'_0$  and  $x'_0$ , are determined by

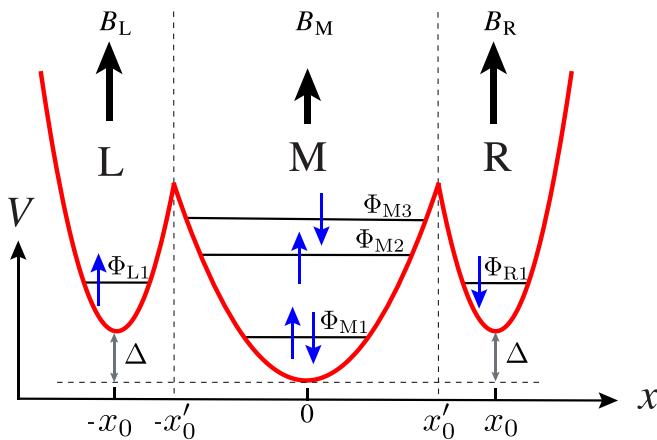


FIG. 2. Schematic illustration of the model potential given in Eq. (3). The dashed lines mark the boundaries between adjacent potential wells.  $\Phi_{\eta j}$  denotes the  $j$ th FD state in dot  $\eta$ , where  $\eta \in \{L, M, R\}$ .

locating the values of  $x$  at which the potential values of dots L and M and dots M and R are equal, respectively, at  $y = 0$ .

We use the CI method to solve the multielectron problem, which involves using a set of predetermined single-electron wave functions. Several methods to obtain the single-electron wave functions exist, including the  $\mathbf{k} \cdot \mathbf{p}$  approximation [67,68], empirical tight binding [69–73], empirical pseudopotential [74–77], and Fock-Darwin (FD) states [78]. In this work, we use the orthonormalized FD states to approximate the single-electron wave functions in a quantum dot. The orthonormalized FD states are obtained with Cholesky decomposition of the overlap matrix formed by the bare FD states [78]. We denote the  $j$ th orthonormalized FD state in dot  $\eta$  as  $\Phi_{\eta j}$  (see Fig. 2). A rigorous description of the multielectron eigenstates requires keeping all the FD states, which is forbiddingly expensive. In practice, one truncates the number of FD states in each quantum dot while maintaining the convergence. Here, we use a cutoff scheme to keep the CI calculation tractable [78]. In this scheme, only the multielectron Slater determinants whose noninteracting energies are within the predefined cutoff values are retained. The cutoff values are defined to be the maximum achievable energy by a Slater determinant with one electron occupying the highest FD state while the remaining electrons occupy the ground orbital. We keep the 10 lowest FD states (corresponding to a principal quantum number  $n$  up to 3) in each dot, as suggested by the convergence of the ground energies of two- and four-electron states in a quantum dot (see Fig. 3) and the convergence of the exchange energy of the two-electron state in an undetuned double-quantum-dot device (see Fig. 4). The calculations for the six-electron system are carried out on a high-performance computing cluster with four hundred eighty 2.2-GHz Intel Xeon CPUs and 42 GB of memory, where a data point at a given detuning  $\Delta$  typically costs 40 min.

### III. RESULTS

#### A. Multielectron single dot

Superexchange interaction allows the spin exchange between two antiparallel spins, each of which occupies dot L and dot R (see Fig. 1). In this work, we evaluate and compare the superexchange interaction mediated by two- and four-electron states in dot M (see Fig. 1). Therefore, understanding the total spin  $S$  of the few-electron ground state in dot M in terms of the magnetic field strength is important in studying the superexchange interaction [79]. The energy and total spin of the ground state for a two- and four-electron system in a QD are discussed in Secs. III A 1 and III A 2, respectively.

##### 1. Two-electron system in a QD

Figure 3(a) shows the ground-state energy of a two-electron system in a QD as a function of the maximum principal quantum number  $n$  of orbitals kept in the CI calculations. Figure 3(a) shows that, for  $n \geq 2$ , convergence is reached for the ground-state energy. Also, the explicit forms of the ground states indicate that the two-electron states form singlet ground states ( $S = 0$ ; see Table I). For example, at  $B = 0.84$  T, the explicit form of the two-electron

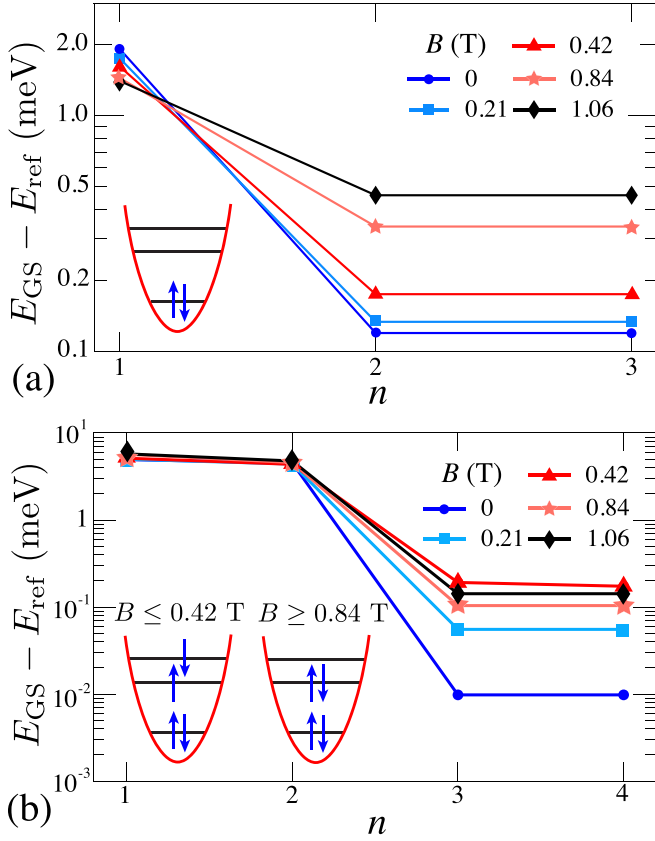


FIG. 3. Ground-state energy of a quantum dot occupied by (a) two electrons and (b) four electrons versus the maximum principal quantum number  $n$  of orbitals kept in the CI calculations. The schematic illustrations of the electron configurations are given in the bottom left corner.  $E_{\text{ref}}$  denotes the reference energy.

ground state is

$$\begin{aligned}
 |\text{GS}\rangle = & 0.885|\uparrow_{M1}\downarrow_{M1}\rangle' \\
 & + 0.233(|\uparrow_{M2}\downarrow_{M3}\rangle' + |\uparrow_{M3}\downarrow_{M2}\rangle') \\
 & - 0.233(|\uparrow_{M1}\downarrow_{M5}\rangle' + |\uparrow_{M5}\downarrow_{M1}\rangle') + \dots, \quad (4)
 \end{aligned}$$

where  $|\uparrow_{\Phi_j}\downarrow_{\Phi_k}\rangle'$  denotes a two-electron Slater determinant with a spin-up electron occupying the FD orbital  $\Phi_j$  while another spin-down electron occupies the FD orbital  $\Phi_k$ . In Eq. (4), the dots ( $\dots$ ) indicate other Slater determinants with smaller magnitudes of coefficients. For low magnetic field strengths, the experimental results that demonstrate a two-electron singlet state as the ground state in a QD conform with the full CI results here [3,10,14,16,24,80–82].

## 2. Four-electron system

Experiments have shown that the total spin of a four-electron ground state in a QD varies depending on the magnitude of the external magnetic field. At a low magnetic field strength, the ground state of a four-electron system in a QD is a triplet,  $S = 1$  [80,81]. In contrast, at a larger magnetic field strength, the four-electron ground state switches to a singlet,  $S = 0$  [80,81].

Figure 3(b) shows the ground-state energy of a four-electron system in a QD as a function of the maximum

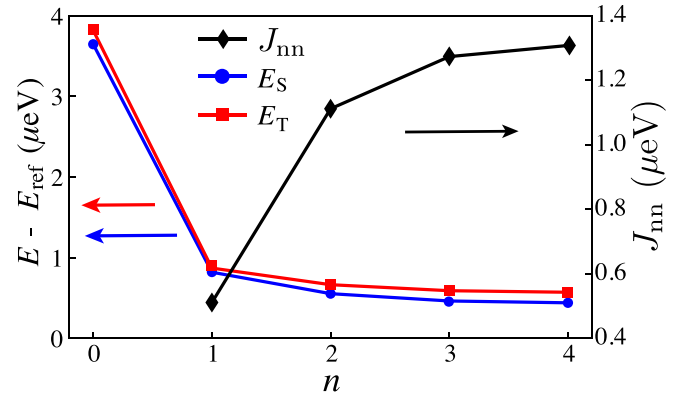


FIG. 4. Lowest singlet (blue circles) and triplet (red squares) eigenvalues and the corresponding exchange energy versus the maximum principal quantum number  $n$  of orbitals kept in the CI calculation. The parameters are interdot distance  $x_0 = 28$  nm,  $\hbar\omega_0 = 7.28$  meV, and  $B = 0.21$  T. The results show that the nearest-neighbor exchange energy  $J_{nn}$  (black diamonds) converges for  $n \geq 3$ .

principal quantum number  $n$  of orbitals kept in the CI calculations. Figure 3(b) shows that, for  $n \geq 3$ , convergence is reached for the ground-state energy. In addition, the explicit forms of the ground states indicate that, for  $B \lesssim 0.42$  T, the ground state is a triplet state ( $S = 1$ ), while for  $B \gtrsim 0.84$  T, the ground state is a singlet state ( $S = 0$ ; see Table I). In particular, at  $B = 0.21$  T, the ground state is a triplet state, whose explicit form is

$$\begin{aligned}
 |\text{GS}\rangle &= 0.576(|\uparrow_{M2}\downarrow_{M3}\uparrow_{M1}\downarrow_{M1}\rangle' - |\uparrow_{M3}\downarrow_{M2}\uparrow_{M1}\downarrow_{M1}\rangle') \\
 &+ [0.204(|\uparrow_{M1}\uparrow_{M3}\downarrow_{M2}\downarrow_{M5}\rangle' - |\uparrow_{M1}\uparrow_{M2}\downarrow_{M3}\downarrow_{M5}\rangle') \\
 &+ 0.204(|\uparrow_{M3}\uparrow_{M5}\downarrow_{M1}\downarrow_{M2}\rangle' - |\uparrow_{M2}\uparrow_{M5}\downarrow_{M1}\downarrow_{M3}\rangle') \\
 &+ 0.016(|\uparrow_{M2}\uparrow_{M3}\downarrow_{M1}\downarrow_{M5}\rangle' - |\uparrow_{M1}\uparrow_{M5}\downarrow_{M2}\downarrow_{M3}\rangle')] \\
 &+ \dots, \quad (5)
 \end{aligned}$$

where  $|\uparrow_{\Phi_j}\downarrow_{\Phi_k}\uparrow_{\Phi_m}\downarrow_{\Phi_n}\rangle'$  denotes a four-electron Slater determinant with two spin-up electrons occupying FD orbitals  $\Phi_j$  and  $\Phi_m$  and two spin-down electrons occupying FD orbitals  $\Phi_k$  and  $\Phi_n$ . On the other hand, at  $B = 0.84$  T, the ground state

TABLE I. Ground-state configuration of a quantum dot occupied by two electrons ( $2e$ ) and four electrons ( $4e$ ) based on the cutoff scheme with varying magnetic field. S indicates a singlet, and T indicates a triplet. The confinement energy of the quantum dot is  $\hbar\omega_0 = 3.64$  meV. Ten orbitals (up to  $n = 3$ ) are retained for the single quantum dot in the CI calculation.

$B$ (T)	Ground-state configuration	
	$2e$	$4e$
0	S	T
0.21	S	T
0.42	S	T
0.84	S	S
1.06	S	S

TABLE II. Eigenstates of the low-energy subspace formed by six electrons when four electrons in dot M form a triplet ground state or a singlet ground state.  $|\uparrow\psi_j\uparrow\psi_k\downarrow\psi_m\downarrow\psi_n\rangle$  ( $|\uparrow\psi_j\downarrow\psi_k\rangle|\uparrow\psi_m\downarrow\psi_n\rangle$ ) denotes a six-electron Slater determinant  $|\uparrow\psi_j\uparrow\psi_k\downarrow\psi_m\downarrow\psi_n\uparrow_{M1}\downarrow_{M1}\rangle$  ( $|\uparrow\psi_j\downarrow\psi_k\uparrow\psi_m\downarrow\psi_n\uparrow_{M1}\downarrow_{M1}\rangle$ ), where electrons occupy the orbitals  $\psi_j$ . To simplify the notation, the spins in the core orbital  $\Psi_{M1}$  are dropped. Note that the orbital  $\Psi_{\eta_j}$  denotes the  $j$ th lowest orbital in dot  $\eta$  and should be perceived as a linear combination of FD orbitals  $\Phi_{\eta_j}$ . The explicit expressions of the eigenstates written in FD orbitals are given in Eq. (B1). The  $S^2$  column shows the eigenvalues of the operator  $S^2$ .

Label	$S^2$	Eigenstates
$ T^0T^1\rangle$	0	$2 \uparrow_{M2}\uparrow_{M3}\downarrow_{R1}\downarrow_{L1}\rangle + 2 \uparrow_{R1}\uparrow_{L1}\downarrow_{M2}\downarrow_{M3}\rangle - ( \uparrow_{R1}\downarrow_{L1}\rangle -  \uparrow_{L1}\downarrow_{R1}\rangle)( \uparrow_{M2}\downarrow_{M3}\rangle -  \uparrow_{M3}\downarrow_{M2}\rangle)$
$ S^0S^1\rangle$	0	$( \uparrow_{R1}\downarrow_{L1}\rangle +  \uparrow_{L1}\downarrow_{R1}\rangle)( \uparrow_{M2}\downarrow_{M3}\rangle +  \uparrow_{M3}\downarrow_{M2}\rangle)$
$ S^0T^1\rangle$	2	$( \uparrow_{R1}\downarrow_{L1}\rangle +  \uparrow_{L1}\downarrow_{R1}\rangle)( \uparrow_{M2}\downarrow_{M3}\rangle -  \uparrow_{M3}\downarrow_{M2}\rangle)$
$ T^0S^1\rangle$	2	$( \uparrow_{R1}\downarrow_{L1}\rangle -  \uparrow_{L1}\downarrow_{R1}\rangle)( \uparrow_{M2}\downarrow_{M3}\rangle +  \uparrow_{M3}\downarrow_{M2}\rangle)$
$ T_{\pm}^0T_{\pm}^1\rangle$	2	$ \uparrow_{M2}\uparrow_{M3}\downarrow_{R1}\downarrow_{L1}\rangle -  \uparrow_{R1}\uparrow_{L1}\downarrow_{M2}\downarrow_{M3}\rangle$
$ T^0T^1\rangle^{(2)}$	6	$ \uparrow_{M2}\uparrow_{M3}\downarrow_{R1}\downarrow_{L1}\rangle +  \uparrow_{R1}\uparrow_{L1}\downarrow_{M2}\downarrow_{M3}\rangle + ( \uparrow_{R1}\downarrow_{L1}\rangle -  \uparrow_{L1}\downarrow_{R1}\rangle)( \uparrow_{M2}\downarrow_{M3}\rangle -  \uparrow_{M3}\downarrow_{M2}\rangle)$

is a singlet state, whose explicit form is

$$\begin{aligned}
 |\text{GS}\rangle = & 0.807|\uparrow_{M1}\downarrow_{M1}\uparrow_{M2}\downarrow_{M2}\rangle' \\
 & + 0.266(|\uparrow_{M1}\downarrow_{M5}\uparrow_{M2}\downarrow_{M2}\rangle' + |\uparrow_{M5}\downarrow_{M1}\uparrow_{M2}\downarrow_{M2}\rangle') \\
 & + 0.234(|\uparrow_{M2}\downarrow_{M8}\uparrow_{M1}\downarrow_{M1}\rangle' + |\uparrow_{M8}\downarrow_{M2}\uparrow_{M1}\downarrow_{M1}\rangle') \\
 & + \dots
 \end{aligned} \quad (6)$$

The results of the full CI calculations presented above conform with the experimental results described in the previous paragraph [80,81].

### B. Multielectron-mediated superexchange $J$

In this section, we present the results of the superexchange energy  $J$  for different cases: In Sec. III B 1,  $J$  mediated by a four-electron triplet state in dot M is discussed. In Sec. III B 2,  $J$  mediated by a four-electron singlet state in dot M is discussed. In Sec. III B 3, in comparison with the results in Secs. III B 1 and III B 2,  $J$  mediated by a two-electron singlet state in dot M is discussed.

We denote the electron occupation of the ground state in each dot as  $(n_L, n_M, n_R)$ , where  $n_L$  ( $n_M, n_R$ ) indicates the number of electrons in dot L (M, R). For descriptive purposes, we denote the ground-state configurations formed by  $n_M$  electrons in dot M as  $|S_{n_M}\rangle$  and  $|T_{n_M}\rangle$  for the singlet and triplet states, respectively. The superexchange energies  $J$  are evaluated at the detuning,  $\Delta$ , such that the number of electrons in dot M is  $n_M$ . For illustrative purposes, throughout this paper, we plot negative  $J$  as dashed lines and positive  $J$  as solid lines.

For a TQD device with six electrons in the (1,4,1) region, two cases exist for the four-electron state in dot M. As suggested by the results based on a single dot (Table I), at weak magnetic fields ( $B \lesssim 0.42$  T), we would expect four electrons in dot M to form a triplet ground state  $|T_4\rangle$ . In this case, as will be discussed in Sec. III B 1, the superexchange interaction is mediated by a four-electron triplet state in dot M [see case (ii) in Fig. 1]. On the other hand, at larger magnetic fields ( $B \gtrsim 0.84$  T), the electrons form a singlet ground state  $|S_4\rangle$ . Therefore, as will be discussed in Sec. III B 2, the superexchange interaction is mediated by a four-electron singlet state in dot M [see case (iii) in Fig. 1].

For a four-electron system in a TQD device, in the (1,2,1) region, two electrons in dot M form a singlet ground state  $|S_2\rangle$ . Therefore, as will be discussed in Sec. III B 3, the

superexchange interaction between two spins in dot L and dot R is mediated by a two-electron singlet state in dot M [see case (i) in Fig. 1].

#### 1. Superexchange interaction mediated by a four-electron triplet state in dot M [case (ii) in Fig. 1]

Table II shows the six eigenstates spanning the low-energy subspace of a six-electron system with  $S_z = 0$  in the (1,4,1) region [see Eq. (B1) for explicit expressions of the eigenstates written in FD orbitals]. As discussed in Sec. III A 2, when a weak magnetic field is applied at dot M ( $B_M \lesssim 0.42$  T), four electrons in dot M form a triplet ground state. In this case, four of the six eigenstates with triplet ground states in dot M yield the lowest energies, i.e.,  $|T^0T^1\rangle$ ,  $|S^0T^1\rangle$ ,  $|T_{\pm}^0T_{\pm}^1\rangle$ , and  $|T^0T^1\rangle^{(2)}$ .

When four electrons in dot M form a triplet state  $|T_4\rangle$ , we denote the logical states of a single-triplet qubit formed by two antiparallel spins in dot L and dot R as

$$\begin{aligned}
 |\tilde{S}\rangle &= (|\uparrow_{R1}\downarrow_{L1}\rangle + |\uparrow_{L1}\downarrow_{R1}\rangle)|T^1\rangle, \\
 |\tilde{T}\rangle &= (|\uparrow_{R1}\downarrow_{L1}\rangle - |\uparrow_{L1}\downarrow_{R1}\rangle)|T^1\rangle
 \end{aligned} \quad (7)$$

and the leakage states as

$$|\tilde{T}_{\pm}\rangle = |\uparrow_{R1}\uparrow_{L1}\rangle|T_{\pm}^1\rangle, \quad |\tilde{T}_{\pm}\rangle = |\downarrow_{R1}\downarrow_{L1}\rangle|T_{\pm}^1\rangle, \quad (8)$$

where

$$\begin{aligned}
 |T^1\rangle &= (|\uparrow_{M2}\downarrow_{M3}\rangle - |\uparrow_{M3}\downarrow_{M2}\rangle)|\uparrow_{M1}\downarrow_{M1}\rangle, \\
 |T_{+}^1\rangle &= |\uparrow_{M2}\uparrow_{M3}\rangle|\uparrow_{M1}\downarrow_{M1}\rangle, \\
 |T_{-}^1\rangle &= |\downarrow_{M2}\downarrow_{M3}\rangle|\uparrow_{M1}\downarrow_{M1}\rangle.
 \end{aligned} \quad (9)$$

The superexchange energy  $J$  is defined as the energy difference between  $|\tilde{S}\rangle$  and  $|\tilde{T}\rangle$ , which is evaluated at the value of  $\Delta$  such that  $n_M = 4$ . When the applied magnetic field is uniform across the TQD, the logical and leakage states are highly mixed, resulting in severe leakage (see Table II). Following the proposal for a pair of exchange-coupled singlet-triplet qubits [83–86], the leakage can be suppressed by applying different magnetic fields on the outer and inner dots, i.e.,  $|\Delta B| = |B_{L/R} - B_M| \gtrsim 0$ . The nonuniform magnetic field splits the energies of  $|\tilde{T}_{\pm}\rangle$  and  $|\tilde{T}\rangle$  away from the energy of  $|\tilde{T}\rangle$  [see Fig. 5(a)]. We found that for parameters relevant to this work, leakage into  $|\tilde{T}_{\pm}\rangle$  is smaller than  $10^{-3}$  for  $B_{L/R} - B_M \gtrsim 0.42$  T [see Fig. 5(b); see Appendix A for the definition of leakage].



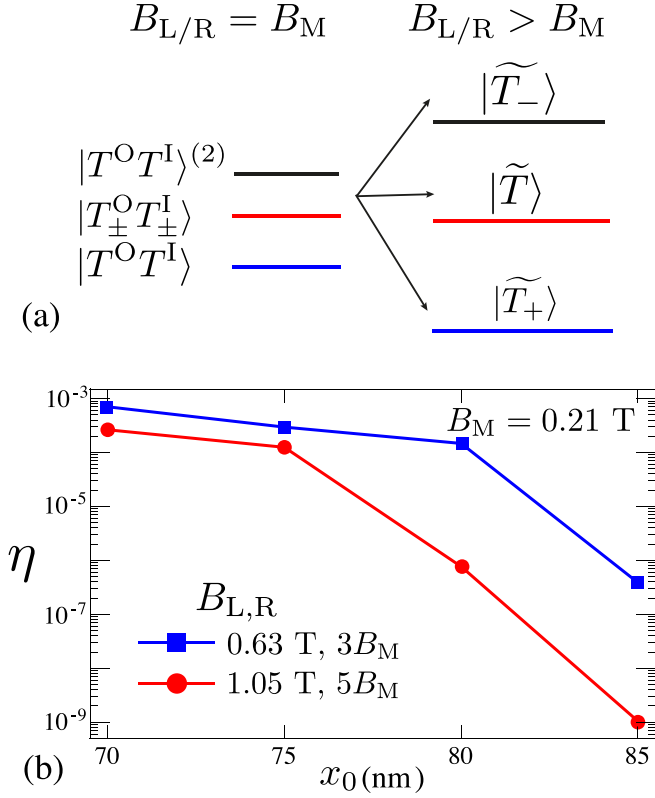


FIG. 5. (a) Schematic illustration of increased splittings between triplet states when the applied magnetic fields on outer dots are stronger,  $B_{L/R} > B_M$ . (b) Leakage  $\eta$  as a function interdot distances  $x_0$  for  $B_{L/R} = 3B_M$  (blue squares) and  $B_{L/R} = 5B_M$  (red circles). A magnetic field of strength  $B_M = 0.21\text{T}$  is applied at dot M. The definition of leakage is provided in Appendix A.

As an example, for  $x_0 = 80\text{ nm}$  and  $B_{L,R} = 5B_M$ , full CI results indicate that the first and second excited eigenstates are the logical triplet state  $|\tilde{T}\rangle$  and singlet state  $|\tilde{S}\rangle$ , respectively. Written explicitly, the logical eigenstates are

$$\begin{aligned}
 |\tilde{T}\rangle = & (|\uparrow_{R1}\downarrow_{L1}\rangle' - |\uparrow_{L1}\downarrow_{R1}\rangle') \\
 & \times \{[0.396(|\uparrow_{M2}\downarrow_{M3}\uparrow_{M1}\downarrow_{M1}\rangle' - |\uparrow_{M3}\downarrow_{M2}\uparrow_{M1}\downarrow_{M1}\rangle')] \\
 & + [0.139(|\uparrow_{M1}\uparrow_{M2}\downarrow_{M3}\downarrow_{M5}\rangle' - |\uparrow_{M1}\uparrow_{M3}\downarrow_{M2}\downarrow_{M5}\rangle')] \\
 & + 0.139(|\uparrow_{M2}\uparrow_{M5}\downarrow_{M1}\downarrow_{M3}\rangle' - |\uparrow_{M3}\uparrow_{M5}\downarrow_{M1}\downarrow_{M2}\rangle')] \\
 & + 0.011(|\uparrow_{M1}\uparrow_{M5}\downarrow_{M2}\downarrow_{M3}\rangle' - |\uparrow_{M2}\uparrow_{M3}\downarrow_{M1}\downarrow_{M5}\rangle')]\} \\
 & + \dots, \tag{10a}
 \end{aligned}$$

$$\begin{aligned}
 |\tilde{S}\rangle = & (|\uparrow_{R1}\downarrow_{L1}\rangle' + |\uparrow_{L1}\downarrow_{R1}\rangle') \\
 & \times \{[0.402(|\uparrow_{M2}\downarrow_{M3}\uparrow_{M1}\downarrow_{M1}\rangle' - |\uparrow_{M3}\downarrow_{M2}\uparrow_{M1}\downarrow_{M1}\rangle')] \\
 & + [0.141(|\uparrow_{M1}\uparrow_{M2}\downarrow_{M3}\downarrow_{M5}\rangle' - |\uparrow_{M1}\uparrow_{M3}\downarrow_{M2}\downarrow_{M5}\rangle')] \\
 & + 0.141(|\uparrow_{M2}\uparrow_{M5}\downarrow_{M1}\downarrow_{M3}\rangle' - |\uparrow_{M3}\uparrow_{M5}\downarrow_{M1}\downarrow_{M2}\rangle')] \\
 & - 0.011(|\uparrow_{M1}\uparrow_{M5}\downarrow_{M2}\downarrow_{M3}\rangle' - |\uparrow_{M2}\uparrow_{M3}\downarrow_{M1}\downarrow_{M5}\rangle')]\} \\
 & + \dots, \tag{10b}
 \end{aligned}$$

where  $|\uparrow_{\phi_j}\downarrow_{\phi_k}\rangle' | \uparrow_{\phi_m}\uparrow_{\phi_n}\downarrow_{\phi_o}\downarrow_{\phi_p}\rangle'$  denotes a six-electron Slater determinant  $|\uparrow_{\phi_j}\downarrow_{\phi_k}\uparrow_{\phi_m}\uparrow_{\phi_n}\downarrow_{\phi_o}\downarrow_{\phi_p}\rangle'$  formed by six

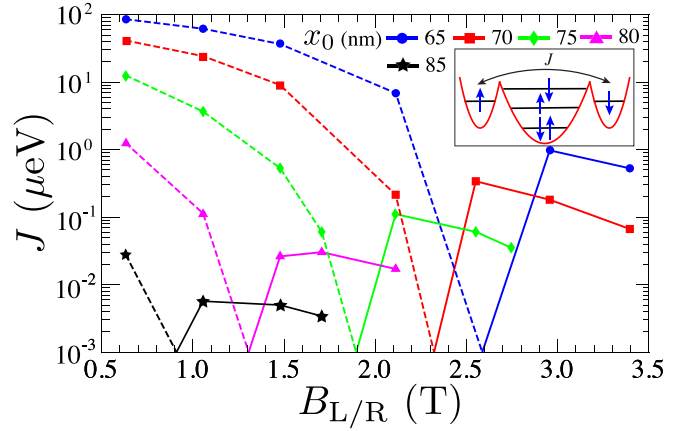


FIG. 6. Superexchange energy  $J$  versus magnetic field applied on outer dots (L and R)  $B_{L/R}$  for a six-electron system. A magnetic field of strength  $B_M = 0.21\text{T}$  is applied at dot M. The inset indicates that the superexchange interaction is mediated by a four-electron triplet state in dot M. Dashed lines represent negative values, and solid lines represent positive values.

electrons occupying the FD orbitals  $\Phi_l$ . In Eq. (10), the linear combinations of four-electron Slater determinants in the curly brackets define a triplet state in dot M.

Figure 6 shows the values of  $J$  as a function of  $B_{L,R}$  for various interdot distances  $x_0$ . As expected, the value of  $|J|$  decreases when the interdot distance increases. Interestingly, the value of  $J$  exhibits a nontrivial behavior when the strength of  $B_{L,R}$  changes. For small  $B_{L,R}$ ,  $J$  is negative, while its magnitude decreases as  $B_{L,R}$  increases. Beyond a certain threshold value of  $B_{L,R}$ ,  $J$  switches sign, becoming positive, and increases as a function of  $B_{L,R}$ . After it reaches a peak

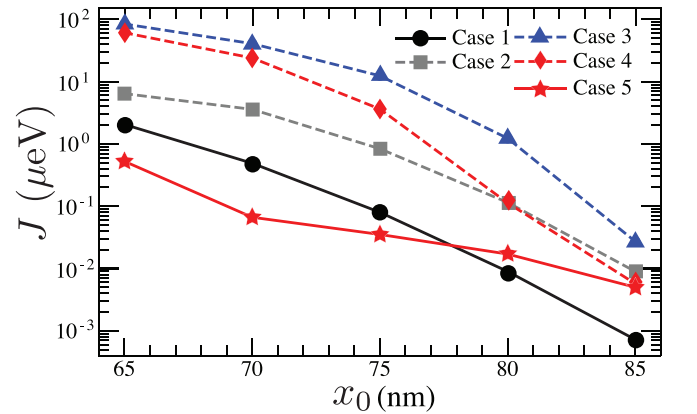


FIG. 7. Absolute value of the superexchange energy  $J$  as a function of interdot distance  $x_0$  for a four-electron system (black circles) and a six-electron system. The values of  $J$  for a six-electron system are divided into four cases based on the electron configurations in the middle dot and the magnetic field on outer dots  $B_{L/R}$ : case 2, four-electron singlet  $|S_4\rangle$  (gray squares); case 3, four-electron triplet  $|T_4\rangle$  and  $B_{L/R} = 3B_M$  (blue triangles); case 4, four-electron triplet  $|T_4\rangle$  and  $B_{L/R} = 5B_M$  (red diamonds); case 5, four-electron triplet  $|T_4\rangle$  and  $B_{L/R} \gg B_M$  (red stars). A summary of the different cases is provided in Table IV. Dashed lines represent negative values, and solid lines represent positive values.

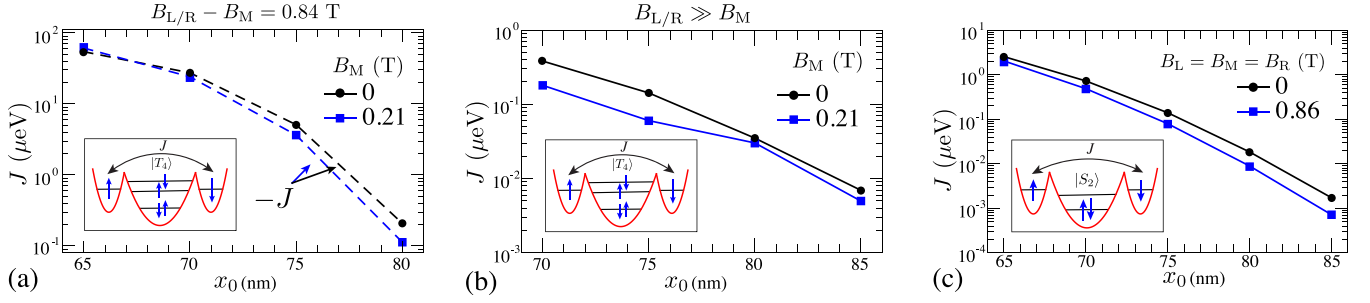


FIG. 8. (a) Four-electron triplet-mediated  $J$  vs  $x_0$  for  $B_{L/R} - B_M = 0.84$  T. The values of  $J$  for  $B_M = 0.21$  T (blue squares) are extracted from Fig. 6. (b) Four-electron triplet-mediated  $J$  vs  $x_0$  for  $B_{L/R} \gg B_M$ . The values of  $J$  for  $B_M = 0.21$  T (blue squares) are extracted from Fig. 6 for  $\Delta B = B_{L/R} - B_M = 2.75$  T (2.33, 1.50, 1.27 T) for  $x_0 = 70$  nm (75, 80, 85 nm). The values of  $J$  for  $B_M = 0$  T are evaluated for the same values of  $\Delta B$ . (c) Two-electron singlet mediated  $J$  vs  $x_0$  for  $B_L = B_M = B_R$ . Dashed lines represent negative values, and solid lines represent positive values.

value, it decreases again but maintains its positive value. The values of  $J$  in Fig. 6 are obtained for  $B_M = 0.21$  T. Switching to the case in which  $B_M = 0$  does not change the main results in an important way [see Figs. 8(a) and 8(b); see Appendix C for details].

In this section, for practical purposes, the results of full CI calculations are obtained by assuming different (discontinuous) magnetic field strengths at different dots, i.e.,  $B_L = B_R \neq B_M$  (see Fig. 2). In experiments, the application of different magnetic field strengths at different dot centers is achieved by employing a proximal micromagnet, which generates a continuous magnetic gradient across the QDs. Together with an external magnetic field, the magnetic gradient gives rise to a nonuniform magnetic field at the dot centers such that  $B_L = B_R > B_M$ . Therefore, away from the dot centers, the presence of the continuous magnetic gradient gives rise to changes in the confinement lengths of the FD orbitals  $l_B$  [87]. However, taking into account the changes in  $l_B$  would result in an intractable calculation path since that requires a purely numerical integration on all the single- and two-particle operators, i.e.,  $\int \Phi_j^* h \Phi_k$  and  $\int \Phi_j^* \Phi_k^* (e^2 / \epsilon |\mathbf{r}_1 - \mathbf{r}_2|) \Phi_m \Phi_n$ , respectively. In addition, for the parameters of concern, the changes in  $l_B$  away from the dot centers are minute and can be safely neglected. Therefore, we expect that the features will be qualitatively similar if the changes in  $l_B$  from the continuous magnetic gradient are included in the CI method.

## 2. Superexchange interaction mediated by a four-electron singlet state in dot M [case (iii) in Fig. 1]

When a larger uniform magnetic field is applied across the TQD device, the lowest logical subspace is free of leakage since four electrons in dot M form a singlet ground state  $|S_4\rangle$ . The logical states are shown in Table III. In this case, the superexchange interaction is mediated by a four-electron singlet  $|S_4\rangle$  in dot M.

Gray squares in Fig. 7 show the values of superexchange interaction mediated by  $|S_4\rangle$  in dot M.  $J$  is evaluated at the value of  $\Delta$  such that  $n_M = 4$ . As an example, for  $x_0 = 80$  nm and  $B_L = B_M = B_R = 0.86$  T, full CI results indicate that the ground and first excited eigenstates are the logical triplet state  $|T\rangle$  and singlet state  $|S\rangle$ , respectively. Written explicitly, the

logical eigenstates are

$$\begin{aligned} |T\rangle &= |T^0 S^1\rangle \\ &= (|\uparrow_{R1} \downarrow_{L1}\rangle' - |\uparrow_{L1} \downarrow_{R1}\rangle') \\ &\quad \times [0.560 |\uparrow_{M2} \downarrow_{M2}\rangle' |\uparrow_{M1} \downarrow_{M1}\rangle' \\ &\quad - 0.182 (|\uparrow_{M1} \downarrow_{M5}\rangle' + |\uparrow_{M5} \downarrow_{M1}\rangle') |\uparrow_{M1} \downarrow_{M1}\rangle' \\ &\quad + \dots], \end{aligned} \quad (11a)$$

$$\begin{aligned} |S\rangle &= |S^0 S^1\rangle \\ &= (|\uparrow_{R1} \downarrow_{L1}\rangle' + |\uparrow_{L1} \downarrow_{R1}\rangle') \\ &\quad \times [-0.560 |\uparrow_{M2} \downarrow_{M2}\rangle' |\uparrow_{M1} \downarrow_{M1}\rangle' \\ &\quad + 0.182 (|\uparrow_{M1} \downarrow_{M5}\rangle' + |\uparrow_{M5} \downarrow_{M1}\rangle') |\uparrow_{M2} \downarrow_{M2}\rangle' \\ &\quad + \dots], \end{aligned} \quad (11b)$$

where  $|\uparrow_{\phi_j} \downarrow_{\phi_k}\rangle' |\uparrow_{\phi_m} \downarrow_{\phi_n}\rangle' |\uparrow_{\phi_o} \downarrow_{\phi_p}\rangle'$  denotes a six-electron Slater determinant  $|\uparrow_{\phi_j} \downarrow_{\phi_k} \uparrow_{\phi_m} \downarrow_{\phi_n} \uparrow_{\phi_o} \downarrow_{\phi_p}\rangle'$  with six electrons occupying the FD orbitals  $\Phi_l$ . In Eq. (11), the linear combinations of four-electron Slater determinants in the square brackets define a singlet state in dot M.

We compare the values of  $J$  mediated by  $|S_4\rangle$  with other cases in the next section.

TABLE III. Eigenstates of the subspace formed by six electrons when four electrons in dot M form a singlet ground state.  $|\uparrow_{\psi_j} \downarrow_{\psi_k}\rangle |\uparrow_{\psi_m} \downarrow_{\psi_n} \uparrow_{\psi_o} \downarrow_{\psi_p}\rangle$  denotes a six-electron Slater determinant  $|\uparrow_{\psi_j} \downarrow_{\psi_k} \uparrow_{\psi_m} \downarrow_{\psi_n} \uparrow_{\psi_o} \downarrow_{\psi_p}\rangle$ , where electrons occupy the orbitals  $\Psi_j$ . Note that the orbital  $\Psi_{\eta j}$  denotes the  $j$ th lowest orbital in dot  $\eta$  and should be perceived as a linear combination of FD orbitals  $\Phi_{\eta j}$ . The explicit expressions for the eigenstates written in FD orbitals are given in Eq. (11). The  $S^2$  column shows the eigenvalues of the operator  $S^2$ .

Label	$S^2$	Eigenstates
$ S^0 S^1\rangle$	0	$( \uparrow_{R1} \downarrow_{L1}\rangle +  \uparrow_{L1} \downarrow_{R1}\rangle)  \uparrow_{M1} \downarrow_{M1} \uparrow_{M2} \downarrow_{M2}\rangle$
$ T^0 S^1\rangle$	2	$( \uparrow_{R1} \downarrow_{L1}\rangle -  \uparrow_{L1} \downarrow_{R1}\rangle)  \uparrow_{M1} \downarrow_{M1} \uparrow_{M2} \downarrow_{M2}\rangle$

TABLE IV. Summary of the different cases in Fig. 7.  $|S_{nM}\rangle$  ( $|T_{nM}\rangle$ ) denotes the singlet (triplet) ground state formed by  $n_M$  electrons in dot M.

Case	$(n_L, n_M, n_R)$	$B_{L/M/R}$ (T)	Ground state in dot M
1	(1,2,1)	$B_{L/M/R} = 0.86$	$ S_2\rangle$
2	(1,4,1)	$B_{L/M/R} = 0.86$	$ S_4\rangle$
3	(1,4,1)	$B_M = 0.21, B_{L/R} = 3B_M$	$ T_4\rangle$
4	(1,4,1)	$B_M = 0.21, B_{L/R} = 5B_M$	$ T_4\rangle$
5	(1,4,1)	$B_{L/R} \gg B_M$	$ T_4\rangle$

### 3. Comparison between two- and four-electro-mediated superexchange [cases (i), (ii), and (iii) in Fig. 1]

Figure 7 shows the value of superexchange energy  $J$  as a function of the interdot distance for several cases, including  $J$  mediated by two electrons [black circles, case (i) in Fig. 1],  $J$  mediated by a four-electron singlet [gray squares, case (iii) in Fig. 1], and  $J$  mediated by a four-electron triplet [blue triangles, red diamonds, and red stars for different  $B_{L/R}$ , case (ii) in Fig. 1]. The data points for the red stars are extracted from Fig. 6 at the second values of  $B_{L/R}$  which give positive  $J$ . The details of the electron configurations for different cases of  $J$  in Fig. 7 are shown in Table IV.

We first focus on the six-electron system. At smaller  $x_0$ ,  $J$  mediated by a four-electron triplet  $|T_4\rangle$  yields a larger magnitude than  $J$  mediated by a four-electron singlet  $|S_4\rangle$ . In particular,  $J$  mediated by  $|T_4\rangle$  with  $B_{L/R} = 3B_M$  yields an absolute value that is around one order of magnitude larger than  $J$  mediated by  $|S_4\rangle$  (compare blue triangles, case 3, and gray squares, case 2, for  $x_0 \lesssim 75$  nm in Fig. 7). On the other hand, at large  $x_0$  ( $x_0 = 85$  nm),  $J$  mediated by  $|S_4\rangle$  and  $|T_4\rangle$  give comparable  $|J|$ .

We next compare  $J$  mediated by two-electron and four-electron states in dot M. Overall, four-electron-mediated  $J$  is stronger than two-electron- ( $|S_2\rangle$ ) mediated  $J$ , except for the case in which  $B_{L,R} \gg B_M$ . In particular,  $|S_4\rangle$ -mediated  $J$  is around one order of magnitude stronger than  $|S_2\rangle$ -mediated  $J$ , while  $|T_4\rangle$ -mediated  $J$  at  $B_{L/R} = 3B_M$  is about two orders of magnitude stronger. Such a magnetic gradient,  $\Delta B = B_{L/R} - B_M = 0.42$  T =  $10 \mu\text{eV} = 2.5$  GHz  $\times h$ , should be achievable in near-term quantum devices [88] since a magnetic gradient as high as  $\Delta B = 1$  GHz has been demonstrated [40]. It should be noted that larger  $J$  can be achieved for  $|S_2\rangle$  at much smaller  $x_0$  [64]. However,  $|S_4\rangle$  or  $|T_4\rangle$  is not achievable in that regime because for small interdot distances, the (1,4,1) dot occupation is not well defined.

## IV. CONCLUSIONS

We have shown, using full CI calculations, that in a TQD device, the variation of the number of electrons in the mediator has a considerable impact on the superexchange. We have observed that the magnitude of superexchange decreases as the interdot distances are increased. We have found that the four-electron mediator yields a stronger superexchange than the two-electron mediator for the same interdot distance in most cases. We have further shown that, in comparison to the four-electron singlet in the mediating dot, the four-electron triplet exhibits stronger superexchange, except when the magnetic field on the outer dots is much stronger than that on the middle dot. Our results therefore should facilitate realization of large-scale architecture with long-range connectivity for a quantum-dot spin qubit.

## ACKNOWLEDGMENTS

We acknowledge support from the Key-Area Research and Development Program of Guangdong Province (Grant No. 2018B030326001), the National Natural Science Foundation of China (Grant No. 11874312), the Research Grants Council of Hong Kong (Grant No. 11303617), and the Guangdong Innovative and Entrepreneurial Research Team Program (Grant No. 2016ZT06D348). The calculations involved in this work were mostly performed on the Tianhe-2 supercomputer at the National Supercomputer Center in Guangzhou, China.

## APPENDIX A: LEAKAGE INDUCED OVER $t_{2\pi}$

In a uniform external magnetic field, the logical singlet  $|\tilde{S}\rangle = |S^0T^1\rangle$  and triplet  $|\tilde{T}\rangle$  states are highly mixed with the leakage states,  $|\tilde{T}\rangle_+$  and  $|\tilde{T}\rangle_-$  (see discussion in Sec. III B 1). To suppress the leakage into  $|\tilde{T}\rangle_+$ ,  $|\tilde{T}\rangle_-$ , a larger  $\Delta B = B_{L/R} - B_M$  is preferable. Also, we have found that the  $\Delta B$ -induced splittings between  $|\tilde{T}\rangle_+$ ,  $|\tilde{T}\rangle_-$ , and  $|\tilde{T}\rangle$  are not straightforward when we take into account the changes in the magnetic-field-induced splittings between the Fock-Darwin (FD) states. To evaluate the leakage, using the CI results, we first identify the compositions of  $|\tilde{T}\rangle_+$ ,  $|\tilde{T}\rangle_-$ , and  $|\tilde{T}\rangle$  in terms of the Slater determinant and the corresponding orthonormalized FD states. Then, we extract the tunneling energies between them by taking  $t_{\tilde{T},\tilde{T}_{\pm}} = \langle \tilde{T} | H | \tilde{T}_{\pm} \rangle$ . Leakage is estimated as

$$\eta = \sum_{j \in \{+, -\}} \langle \tilde{T}_j | \exp \left\{ -i \left[ \frac{J}{2} (|\tilde{T}\rangle \langle \tilde{T}| - |S^0T^1\rangle \langle S^0T^1|) + t_{\tilde{T},\tilde{T}_j} (|\tilde{T}\rangle \langle \tilde{T}_j| + \text{H.c.}) \right] t_{2\pi} \right\} | \tilde{T} \rangle, \quad (\text{A1})$$

where  $t_{2\pi} = 2\pi \hbar / J$  and  $J = \langle \tilde{T} | H | \tilde{T} \rangle - \langle S^0T^1 | H | S^0T^1 \rangle$ . The resultant leakage is shown in Fig. 5(b).

## APPENDIX B: EIGENSTATES OBTAINED FROM CI CALCULATIONS FOR A SIX-ELECTRON SYSTEM IN THE (1, 4, 1) REGION $B_L = B_M = B_R = 0.21$ T

For  $x_0 = 75$  nm and  $B_L = B_M = B_R = 0.21$  T, the results of CI calculations show that six the lowest eigenstates, written explicitly as linear combinations of six-electron Slater determinants, are

$$\begin{aligned} |T^0T^1\rangle = & 0.226(2|\uparrow_{M2}\uparrow_{M3}\downarrow_{R1}\downarrow_{L1}\rangle' + 2|\uparrow_{R1}\uparrow_{L1}\downarrow_{M2}\downarrow_{M3}\rangle' - |\uparrow_{L1}\uparrow_{M2}\downarrow_{R1}\downarrow_{M3}\rangle' - |\uparrow_{R1}\uparrow_{M2}\downarrow_{L1}\downarrow_{M3}\rangle' \\ & + |\uparrow_{R1}\uparrow_{M2}\downarrow_{L1}\downarrow_{M3}\rangle' + |\uparrow_{L1}\uparrow_{M3}\downarrow_{R1}\downarrow_{M2}\rangle')|\uparrow_{M1}\downarrow_{M1}\rangle' \end{aligned}$$

$$\begin{aligned}
 & + 0.104(2|\uparrow_{M1}\uparrow_{M6}\downarrow_{R1}\downarrow_{L1}\rangle' + 2|\uparrow_{R1}\uparrow_{L1}\downarrow_{M1}\downarrow_{M6}\rangle' - |\uparrow_{L1}\uparrow_{M1}\downarrow_{R1}\downarrow_{M6}\rangle' - |\uparrow_{R1}\uparrow_{M6}\downarrow_{L1}\downarrow_{M1}\rangle' \\
 & + |\uparrow_{R1}\uparrow_{M1}\downarrow_{L1}\downarrow_{M6}\rangle' + |\uparrow_{L1}\uparrow_{M6}\downarrow_{R1}\downarrow_{M1}\rangle')|\uparrow_{M2}\downarrow_{M2}\rangle' + \dots, \tag{B1a}
 \end{aligned}$$

$$\begin{aligned}
 |T_{\pm}^O T_{\pm}^I\rangle & = 0.555(|\uparrow_{R1}\uparrow_{L1}\downarrow_{M2}\downarrow_{M3}\rangle' - |\uparrow_{M2}\uparrow_{M3}\downarrow_{R1}\downarrow_{L1}\rangle')|\uparrow_{M1}\downarrow_{M1}\rangle' \\
 & - 0.127(|\uparrow_{R1}\uparrow_{L1}\downarrow_{M1}\downarrow_{M4}\rangle' - |\uparrow_{M1}\uparrow_{M4}\downarrow_{R1}\downarrow_{L1}\rangle')|\uparrow_{M3}\downarrow_{M3}\rangle' \\
 & + 0.127(|\uparrow_{R1}\uparrow_{L1}\downarrow_{M1}\downarrow_{M6}\rangle' - |\uparrow_{M1}\uparrow_{M6}\downarrow_{R1}\downarrow_{L1}\rangle')|\uparrow_{M2}\downarrow_{M2}\rangle' + \dots, \tag{B1b}
 \end{aligned}$$

$$\begin{aligned}
 |S^O T^I\rangle & = -0.395(|\uparrow_{R1}\uparrow_{M3}\downarrow_{L1}\downarrow_{M2}\rangle' + |\uparrow_{L1}\uparrow_{M3}\downarrow_{R1}\downarrow_{M2}\rangle' - |\uparrow_{L1}\uparrow_{M2}\downarrow_{R1}\downarrow_{M3}\rangle' - |\uparrow_{R1}\uparrow_{M2}\downarrow_{L1}\downarrow_{M3}\rangle')|\uparrow_{M1}\downarrow_{M1}\rangle' \\
 & - 0.091(|\uparrow_{R1}\uparrow_{M4}\downarrow_{L1}\downarrow_{M1}\rangle' + |\uparrow_{L1}\uparrow_{M4}\downarrow_{R1}\downarrow_{M1}\rangle' - |\uparrow_{L1}\uparrow_{M1}\downarrow_{R1}\downarrow_{M4}\rangle' - |\uparrow_{R1}\uparrow_{M1}\downarrow_{L1}\downarrow_{M4}\rangle')|\uparrow_{M3}\downarrow_{M3}\rangle' + \dots, \tag{B1c}
 \end{aligned}$$

$$\begin{aligned}
 |T^O T^I\rangle^{(2)} & = -0.324(|\uparrow_{R1}\uparrow_{M3}\downarrow_{L1}\downarrow_{M2}\rangle' + |\uparrow_{L1}\uparrow_{M2}\downarrow_{R1}\downarrow_{M3}\rangle' + |\uparrow_{R1}\uparrow_{L1}\downarrow_{M2}\downarrow_{M3}\rangle' + |\uparrow_{M2}\uparrow_{M3}\downarrow_{R1}\downarrow_{L1}\rangle' \\
 & - |\uparrow_{L1}\uparrow_{M3}\downarrow_{R1}\downarrow_{M2}\rangle' - |\uparrow_{R1}\uparrow_{M2}\downarrow_{L1}\downarrow_{M3}\rangle')|\uparrow_{M1}\downarrow_{M1}\rangle' \\
 & - 0.074(|\uparrow_{R1}\uparrow_{M4}\downarrow_{L1}\downarrow_{M1}\rangle' + |\uparrow_{L1}\uparrow_{M1}\downarrow_{R1}\downarrow_{M4}\rangle' + |\uparrow_{R1}\uparrow_{L1}\downarrow_{M1}\downarrow_{M4}\rangle' + |\uparrow_{M1}\uparrow_{M4}\downarrow_{R1}\downarrow_{L1}\rangle' \\
 & - |\uparrow_{L1}\uparrow_{M4}\downarrow_{R1}\downarrow_{M1}\rangle' - |\uparrow_{R1}\uparrow_{M1}\downarrow_{L1}\downarrow_{M4}\rangle')|\uparrow_{M3}\downarrow_{M3}\rangle' + \dots, \tag{B1d}
 \end{aligned}$$

$$\begin{aligned}
 |S^O S^I\rangle & = -0.519(|\uparrow_{L1}\downarrow_{R1}\uparrow_{M2}\downarrow_{M2}\rangle' + |\uparrow_{R1}\downarrow_{L1}\uparrow_{M2}\downarrow_{M2}\rangle')|\uparrow_{M1}\downarrow_{M1}\rangle' \\
 & - 0.166(|\uparrow_{L1}\downarrow_{R1}\uparrow_{M5}\downarrow_{M1}\rangle' + |\uparrow_{R1}\downarrow_{L1}\uparrow_{M5}\downarrow_{M1}\rangle' + |\uparrow_{L1}\downarrow_{R1}\uparrow_{M1}\downarrow_{M5}\rangle' + |\uparrow_{R1}\downarrow_{L1}\uparrow_{M1}\downarrow_{M5}\rangle')|\uparrow_{M2}\downarrow_{M2}\rangle' + \dots, \tag{B1e}
 \end{aligned}$$

$$\begin{aligned}
 |T^O S^I\rangle & = 0.520(|\uparrow_{L1}\downarrow_{R1}\uparrow_{M2}\downarrow_{M2}\rangle' - |\uparrow_{R1}\downarrow_{L1}\uparrow_{M2}\downarrow_{M2}\rangle')|\uparrow_{M1}\downarrow_{M1}\rangle' \\
 & + 0.166(|\uparrow_{L1}\downarrow_{R1}\uparrow_{M5}\downarrow_{M1}\rangle' + |\uparrow_{R1}\downarrow_{L1}\uparrow_{M5}\downarrow_{M1}\rangle' + |\uparrow_{L1}\downarrow_{R1}\uparrow_{M1}\downarrow_{M5}\rangle' + |\uparrow_{R1}\downarrow_{L1}\uparrow_{M1}\downarrow_{M5}\rangle')|\uparrow_{M2}\downarrow_{M2}\rangle' + \dots, \tag{B1f}
 \end{aligned}$$

where  $|\uparrow_{\Phi_j}\uparrow_{\Phi_k}\downarrow_{\Phi_m}\downarrow_{\Phi_n}\rangle'|\uparrow_{\Phi_o}\downarrow_{\Phi_p}\rangle'$  denotes a six-electron Slater determinant  $|\uparrow_{\Phi_j}\uparrow_{\Phi_k}\downarrow_{\Phi_m}\downarrow_{\Phi_n}\uparrow_{\Phi_o}\downarrow_{\Phi_p}\rangle'$  in which three spin-up (spin-down) electrons occupy the FD orbitals  $\Phi_j$ ,  $\Phi_k$ , and  $\Phi_o$  ( $\Phi_m$ ,  $\Phi_n$ , and  $\Phi_p$ ). In Eq. (B1), the dots ( $\dots$ ) denote other Slater determinants whose coefficients exhibit smaller magnitudes compared to those explicitly shown. The eigenvalue of the operator  $S^2$  for the eigenstate labeled  $|T^O T^I\rangle$  ( $|T_{\pm}^O T_{\pm}^I\rangle$ ,  $|S^O T^I\rangle$ ,  $|T^O T^I\rangle^{(2)}$ ,  $|S^O S^I\rangle$ ,  $|T^O S^I\rangle$ ) is 0 (2, 2, 6, 0, 2).

### APPENDIX C: SUPEREXCHANGE ENERGY $J$ AT THE ZERO EXTERNAL MAGNETIC FIELD

Figure 8 shows the superexchange energy  $J$  evaluated at  $B_M = 0$  and  $B_M = 0.21$  T. Overall, compared to the case in which  $B_M = 0.21$  T, the magnitude of  $J$  is larger for  $B_M = 0$ . However, the main qualitative behaviors of  $J$ , including the order of magnitude and the sign of  $J$ , are the same for both  $B_M = 0$  T and  $B_M = 0.21$  T.

- 
- [1] J. Levy, *Phys. Rev. Lett.* **89**, 147902 (2002).  
 [2] T. Hayashi, T. Fujisawa, H. D. Cheong, Y. H. Jeong, and Y. Hirayama, *Phys. Rev. Lett.* **91**, 226804 (2003).  
 [3] J. R. Petta, A. C. Johnson, J. M. Taylor, E. A. Laird, A. Yacoby, M. D. Lukin, C. M. Marcus, M. P. Hanson, and A. C. Gossard, *Science* **309**, 2180 (2005).  
 [4] B. Krause, T. H. Metzger, A. Rastelli, R. Songmuang, S. Kiravittaya, and O. G. Schmidt, *Phys. Rev. B* **72**, 085339 (2005).  
 [5] J. Gorman, D. G. Hasko, and D. A. Williams, *Phys. Rev. Lett.* **95**, 090502 (2005).  
 [6] G. Shinkai, T. Hayashi, T. Ota, and T. Fujisawa, *Phys. Rev. Lett.* **103**, 056802 (2009).  
 [7] K. D. Petersson, J. R. Petta, H. Lu, and A. C. Gossard, *Phys. Rev. Lett.* **105**, 246804 (2010).  
 [8] E. A. Laird, J. M. Taylor, D. P. DiVincenzo, C. M. Marcus, M. P. Hanson, and A. C. Gossard, *Phys. Rev. B* **82**, 075403 (2010).  
 [9] C. Barthel, J. Medford, C. M. Marcus, M. P. Hanson, and A. C. Gossard, *Phys. Rev. Lett.* **105**, 266808 (2010).  
 [10] Z. Shi, C. B. Simmons, J. R. Prance, J. King Gamble, M. Friesen, D. E. Savage, M. G. Lagally, S. N. Coppersmith, and M. A. Eriksson, *Appl. Phys. Lett.* **99**, 233108 (2011).  
 [11] Y. Dovzhenko, J. Stehlik, K. D. Petersson, J. R. Petta, H. Lu, and A. C. Gossard, *Phys. Rev. B* **84**, 161302(R) (2011).  
 [12] B. M. Maune, M. G. Borselli, B. Huang, T. D. Ladd, P. W. Deelman, K. S. Holabird, A. A. Kiselev, I. Alvarado-Rodriguez, R. S. Ross, A. E. Schmitz, M. Sokolich, C. A. Watson, M. F. Gyure, and A. T. Hunter, *Nature (London)* **481**, 344 (2012).  
 [13] C. Wolpert, L. Wang, A. Rastelli, O. G. Schmidt, H. Giessen, and M. Lippitz, *Phys. Status Solidi B* **249**, 731 (2012).  
 [14] M. D. Shulman, O. E. Dial, S. P. Harvey, H. Bluhm, V. Umansky, and A. Yacoby, *Science* **336**, 202 (2012).  
 [15] Z. Shi, C. B. Simmons, D. R. Ward, J. R. Prance, R. T. Mohr, T. S. Koh, J. K. Gamble, X. Wu, D. E. Savage, M. G. Lagally, M. Friesen, S. N. Coppersmith, and M. A. Eriksson, *Phys. Rev. B* **88**, 075416 (2013).  
 [16] X. Wu, D. R. Ward, J. R. Prance, D. Kim, J. K. Gamble, R. T. Mohr, Z. Shi, D. E. Savage, M. G. Lagally, M. Friesen, S. N.



- Coppersmith, and M. A. Eriksson, *Proc. Natl. Acad. Sci. USA* **111**, 11938 (2014).
- [17] K. Eng, T. D. Ladd, A. Smith, M. G. Borselli, A. A. Kiselev, B. H. Fong, K. S. Holabird, T. M. Hazard, B. Huang, P. W. Deelman, I. Milosavljevic, A. E. Schmitz, R. S. Ross, M. F. Gyure, and A. T. Hunter, *Sci. Adv.* **1**, e1500214 (2015).
- [18] M. D. Reed, B. M. Maune, R. W. Andrews, M. G. Borselli, K. Eng, M. P. Jura, A. A. Kiselev, T. D. Ladd, S. T. Merkel, I. Milosavljevic, E. J. Pritchett, M. T. Rakher, R. S. Ross, A. E. Schmitz, A. Smith, J. A. Wright, M. F. Gyure, and A. T. Hunter, *Phys. Rev. Lett.* **116**, 110402 (2016).
- [19] F. Martins, F. K. Malinowski, P. D. Nissen, E. Barnes, S. Fallahi, G. C. Gardner, M. J. Manfra, C. M. Marcus, and F. Kuemmeth, *Phys. Rev. Lett.* **116**, 116801 (2016).
- [20] P. Harvey-Collard, R. M. Jock, N. T. Jacobson, A. D. Baczewski, A. M. Mounce, M. J. Curry, D. R. Ward, J. M. Anderson, R. P. Manginell, J. R. Wendt, M. Rudolph, T. Pluym, M. P. Lilly, M. Pioro-Ladrière, and M. S. Carroll, in *Proceedings of the 2017 IEEE International Electron Devices Meeting (IEDM)* (IEEE, New York, 2017), pp. 36.5.1–36.5.4.
- [21] F. K. Malinowski, F. Martins, P. D. Nissen, S. Fallahi, G. C. Gardner, M. J. Manfra, C. M. Marcus, and F. Kuemmeth, *Phys. Rev. B* **96**, 045443 (2017).
- [22] A. Noiri, T. Nakajima, J. Yoneda, M. R. Delbecq, P. Stano, T. Otsuka, K. Takeda, S. Amaha, G. Allison, K. Kawasaki, Y. Kojima, A. Ludwig, A. D. Wieck, D. Loss, and S. Tarucha, *Nat. Commun.* **9**, 5066 (2018).
- [23] K. Takeda, A. Noiri, J. Yoneda, T. Nakajima, and S. Tarucha, *Phys. Rev. Lett.* **124**, 117701 (2020).
- [24] P. Cerfontaine, T. Botzem, J. Ritzmann, S. S. Humpohl, A. Ludwig, D. Schuh, D. Bougeard, A. D. Wieck, and H. Bluhm, *Nat. Commun.* **11**, 4144 (2020).
- [25] G. Burkard, D. Loss, and D. P. DiVincenzo, *Phys. Rev. B* **59**, 2070 (1999).
- [26] V. Krápek, P. Klenovský, A. Rastelli, O. G. Schmidt, and D. Munzar, *J. Phys.: Conf. Ser.* **245**, 012027 (2010).
- [27] J. Medford, J. Beil, J. M. Taylor, E. I. Rashba, H. Lu, A. C. Gossard, and C. M. Marcus, *Phys. Rev. Lett.* **111**, 050501 (2013).
- [28] J. M. Taylor, V. Srinivasa, and J. Medford, *Phys. Rev. Lett.* **111**, 050502 (2013).
- [29] X.-C. Yang and X. Wang, *Phys. Rev. A* **96**, 012318 (2017).
- [30] X.-C. Yang and X. Wang, *Phys. Rev. A* **97**, 012304 (2018).
- [31] Y.-P. Shim and C. Tahan, *Phys. Rev. B* **97**, 155402 (2018).
- [32] J. C. Abadillo-Uriel, M. A. Eriksson, S. N. Coppersmith, and M. Friesen, *Nat. Commun.* **10**, 5641 (2019).
- [33] W.-X. Xie, C. Zhang, and Z.-Y. Xue, *Ann. Phys. (Berlin, Ger.)* **533**, 2100054 (2021).
- [34] P. Klenovský, V. Krápek, and J. Humlíček, *Acta Phys. Pol. A* **129**, A-62 (2016).
- [35] M. Friesen, J. Ghosh, M. A. Eriksson, and S. N. Coppersmith, *Nat. Commun.* **8**, 15923 (2017).
- [36] A. Sala and J. Danon, *Phys. Rev. B* **95**, 241303(R) (2017).
- [37] C. Zhang, X.-C. Yang, and X. Wang, *Phys. Rev. A* **97**, 042326 (2018).
- [38] J. Fei, D. Zhou, Y.-P. Shim, S. Oh, X. Hu, and M. Friesen, *Phys. Rev. A* **86**, 062328 (2012).
- [39] H.-O. Li, G. Cao, G.-D. Yu, M. Xiao, G.-C. Guo, H.-W. Jiang, and G.-P. Guo, *Nat. Commun.* **6**, 7681 (2015).
- [40] J. M. Nichol, L. A. Orona, S. P. Harvey, S. Fallahi, G. C. Gardner, M. J. Manfra, and A. Yacoby, *npj Quantum Inf.* **3**, 3 (2017).
- [41] S. F. Neyens, E. R. MacQuarrie, J. P. Dodson, J. Corrigan, N. Holman, B. Thorgrimsson, M. Palma, T. McJunkin, L. F. Edge, M. Friesen, S. N. Coppersmith, and M. A. Eriksson, *Phys. Rev. Applied* **12**, 064049 (2019).
- [42] J. Yun, J. Park, H. Jang, J. Kim, W. Jang, Y. Song, M.-K. Cho, H. Sohn, H. Jung, V. Umansky, and D. Kim, *arXiv:2206.04321* (2022).
- [43] X. Mi, J. V. Cady, D. M. Zajac, P. W. Deelman, and J. R. Petta, *Science* **355**, 156 (2017).
- [44] X. Mi, J. V. Cady, D. M. Zajac, J. Stehlik, L. F. Edge, and J. R. Petta, *Appl. Phys. Lett.* **110**, 043502 (2017).
- [45] X. Mi, M. Benito, S. Putz, D. M. Zajac, J. M. Taylor, G. Burkard, and J. R. Petta, *Nature (London)* **555**, 599 (2018).
- [46] D. J. van Woerkom, P. Scarlino, J. H. Ungerer, C. Müller, J. V. Koski, A. J. Landig, C. Reichl, W. Wegscheider, T. Ihn, K. Ensslin, and A. Wallraff, *Phys. Rev. X* **8**, 041018 (2018).
- [47] J. V. Koski, A. J. Landig, M. Russ, J. C. Abadillo-Uriel, P. Scarlino, B. Kratochwil, C. Reichl, W. Wegscheider, G. Burkard, M. Friesen, S. N. Coppersmith, A. Wallraff, K. Ensslin, and T. Ihn, *Nat. Phys.* **16**, 642 (2020).
- [48] F. Borjans, X. G. Croot, X. Mi, M. J. Gullans, and J. R. Petta, *Nature (London)* **577**, 195 (2020).
- [49] G. Burkard, M. J. Gullans, X. Mi, and J. R. Petta, *Nat. Rev. Phys.* **2**, 129 (2020).
- [50] F. Borjans, X. Croot, S. Putz, X. Mi, S. M. Quinn, A. Pan, J. Kerckhoff, E. J. Pritchett, C. A. Jackson, L. F. Edge, R. S. Ross, T. D. Ladd, M. G. Borselli, M. F. Gyure, and J. R. Petta, *Appl. Phys. Lett.* **116**, 234001 (2020).
- [51] B. Kratochwil, J. V. Koski, A. J. Landig, P. Scarlino, J. C. Abadillo-Uriel, C. Reichl, S. N. Coppersmith, W. Wegscheider, M. Friesen, A. Wallraff, T. Ihn, and K. Ensslin, *Phys. Rev. Research* **3**, 013171 (2021).
- [52] T. Nakajima, M. R. Delbecq, T. Otsuka, S. Amaha, J. Yoneda, A. Noiri, K. Takeda, G. Allison, A. Ludwig, A. D. Wieck, X. Hu, F. Nori, and S. Tarucha, *Nat. Commun.* **9**, 2133 (2018).
- [53] T. Fujita, T. A. Baart, C. Reichl, W. Wegscheider, and L. M. K. Vandersypen, *npj Quantum Inf.* **3**, 22 (2017).
- [54] B. Jadot, P.-A. Mortemousque, E. Chanrion, V. Thiney, A. Ludwig, A. D. Wieck, M. Urdampilleta, C. Bäuerle, and T. Meunier, *Nat. Nanotechnol.* **16**, 570 (2021).
- [55] A. R. Mills, D. M. Zajac, M. J. Gullans, F. J. Schupp, T. M. Hazard, and J. R. Petta, *Nat. Commun.* **10**, 1063 (2019).
- [56] B. Buonacorsi, B. Shaw, and J. Baugh, *Phys. Rev. B* **102**, 125406 (2020).
- [57] F. Ginzler, A. R. Mills, J. R. Petta, and G. Burkard, *Phys. Rev. B* **102**, 195418 (2020).
- [58] K. W. Chan, H. Sahasrabudhe, W. Huang, Y. Wang, H. C. Yang, M. Veldhorst, J. C. C. Hwang, F. A. Mohiyaddin, F. E. Hudson, K. M. Itoh, A. Saraiva, A. Morello, A. Laucht, R. Rahman, and A. S. Dzurak, *Nano Lett.* **21**, 1517 (2021).
- [59] H. Qiao, Y. P. Kandel, S. Fallahi, G. C. Gardner, M. J. Manfra, X. Hu, and J. M. Nichol, *Phys. Rev. Lett.* **126**, 017701 (2021).
- [60] F. K. Malinowski, F. Martins, T. B. Smith, S. D. Bartlett, A. C. Doherty, P. D. Nissen, S. Fallahi, G. C. Gardner, M. J. Manfra, C. M. Marcus, and F. Kuemmeth, *Nat. Commun.* **10**, 1196 (2019).

- [61] T. A. Baart, T. Fujita, C. Reichl, W. Wegscheider, and L. M. K. Vandersypen, *Nat. Nanotechnol.* **12**, 26 (2017).
- [62] H. Qiao, Y. P. Kandel, K. Deng, S. Fallahi, G. C. Gardner, M. J. Manfra, E. Barnes, and J. M. Nichol, *Phys. Rev. X* **10**, 031006 (2020).
- [63] F. R. Braakman, P. Barthelemy, C. Reichl, W. Wegscheider, and L. M. K. Vandersypen, *Nat. Nanotechnol.* **8**, 432 (2013).
- [64] K. Deng and E. Barnes, *Phys. Rev. B* **102**, 035427 (2020).
- [65] It has been theoretically demonstrated that the total spin of a four-electron system in a QD varies depending on the eccentricity of the confining potential [89]. However, evaluating superexchange interaction mediated by a four-electron elliptical mediator with different eccentricities and magnetic field strengths is out of the scope of this work.
- [66] E. Nielsen, E. Barnes, J. P. Kestner, and S. Das Sarma, *Phys. Rev. B* **88**, 195131 (2013).
- [67] B. A. Foreman, *Phys. Rev. B* **56**, R12748 (1997).
- [68] P. Klenovský, A. Schliwa, and D. Bimberg, *Phys. Rev. B* **100**, 115424 (2019).
- [69] T. B. Boykin, G. Klimeck, M. Friesen, S. N. Coppersmith, P. von Allmen, F. Oyafuso, and S. Lee, *Phys. Rev. B* **70**, 165325 (2004).
- [70] T. B. Boykin, G. Klimeck, M. A. Eriksson, M. Friesen, S. N. Coppersmith, P. von Allmen, F. Oyafuso, and S. Lee, *Appl. Phys. Lett.* **84**, 115 (2004).
- [71] M. Friesen and S. N. Coppersmith, *Phys. Rev. B* **81**, 115324 (2010).
- [72] J. C. Abadillo-Uriel, B. Thorgrimsson, D. Kim, L. W. Smith, C. B. Simmons, D. R. Ward, R. H. Foote, J. Corrigan, D. E. Savage, M. G. Lagally, M. J. Calderón, S. N. Coppersmith, M. A. Eriksson, and M. Friesen, *Phys. Rev. B* **98**, 165438 (2018).
- [73] H. E. Ercan, S. N. Coppersmith, and M. Friesen, *Phys. Rev. B* **104**, 235302 (2021).
- [74] A. Zunger, *Phys. Stat. Sol. B* **224**, 727 (2001).
- [75] N. B. Nguyen, C. Dufour, and S. Petit, *J. Phys.: Condens. Matter* **20**, 455209 (2008).
- [76] J.-W. Luo, G. Bester, and A. Zunger, *Phys. Rev. B* **79**, 125329 (2009).
- [77] E. G. Barbagiovanni, L. V. Goncharova, and P. J. Simpson, *Phys. Rev. B* **83**, 035112 (2011).
- [78] E. Barnes, J. P. Kestner, N. T. T. Nguyen, and S. Das Sarma, *Phys. Rev. B* **84**, 235309 (2011).
- [79] An example of the effect of the total spin of a multielectron state on the behavior of the exchange energy was demonstrated in experiments in Ref. [90]. In Ref. [90], the sign of the exchange energy between a singly occupied dot and a multielectron dot varied depending on the total spin of the multielectron ground state.
- [80] L. P. Kouwenhoven, T. H. Oosterkamp, M. W. S. Danoastro, M. Eto, D. G. Austing, T. Honda, and S. Tarucha, *Science* **278**, 1788 (1997).
- [81] S. Kalliakos, M. Rontani, V. Pellegrini, C. P. García, A. Pinczuk, G. Goldoni, E. Molinari, L. N. Pfeiffer, and K. W. West, *Nat. Phys.* **4**, 467 (2008).
- [82] O. E. Dial, M. D. Shulman, S. P. Harvey, H. Bluhm, V. Umansky, and A. Yacoby, *Phys. Rev. Lett.* **110**, 146804 (2013).
- [83] R. Li, X. Hu, and J. Q. You, *Phys. Rev. B* **86**, 205306 (2012).
- [84] M. P. Wardrop and A. C. Doherty, *Phys. Rev. B* **90**, 045418 (2014).
- [85] P. Cerfontaine, R. Otten, M. A. Wolfe, P. Bethke, and H. Bluhm, *Phys. Rev. B* **101**, 155311 (2020).
- [86] D. Buterakos, R. E. Throckmorton, and S. Das Sarma, *Phys. Rev. B* **98**, 035406 (2018).
- [87] The confinement length is  $l_b^2 = l_0^2 / \sqrt{1 + e^2 B^2 l_0^4 / 4\hbar^2}$ , where  $l_0 = \sqrt{\hbar / m^* \omega_0}$ .
- [88] S. Chesi, Y.-D. Wang, J. Yoneda, T. Otsuka, S. Tarucha, and D. Loss, *Phys. Rev. B* **90**, 235311 (2014).
- [89] K. Deng, F. A. Calderon-Vargas, N. J. Mayhall, and E. Barnes, *Phys. Rev. B* **97**, 245301 (2018).
- [90] F. K. Malinowski, F. Martins, T. B. Smith, S. D. Bartlett, A. C. Doherty, P. D. Nissen, S. Fallahi, G. C. Gardner, M. J. Manfra, C. M. Marcus, and F. Kueemeth, *Phys. Rev. X* **8**, 011045 (2018).